On the stochastic dynamics of a nonlinear vibration energy harvester driven by Lévy flight excitations

S U B R A M A N I A N   R A M A K R I S H N A N[1], C O N N O R   E D L U N D[2]
and C O L L I N   L A M B R E C H T[1]

[1]*Department of Mechanical and Industrial Engineering, University of Minnesota Duluth, Duluth, MN 55811, USA*
email: *sramakri@d.umn.edu*
[2]*Department of Electrical Engineering, University of Minnesota Duluth, Duluth, MN 55811, USA*
emails: *edlun065@d.umn.edu; lambr035@umn.edu*

Vibration energy harvesting aims to harness the energy of ambient random vibrations for power generation, particularly in small-scale devices. Typically, stochastic excitation driving the harvester is modelled as a Brownian process and the dynamics are studied in the equilibrium state. However, non-Brownian excitations are of interest, particularly in the nonequilibrium regime of the dynamics. In this work we study the nonequilibrium dynamics of a generic piezoelectric harvester driven by Brownian as well as (non-Brownian) Lévy flight excitation, both in the linear and the Duffing regimes. Both the monostable and the bistable cases of the Duffing regime are studied. The first set of results demonstrate that Lévy flight excitation results in higher expectation values of harvested power. In particular, it is shown that increasing the noise intensity leads to a significant increase in power output. It is also shown that a linearly coupled array of nonlinear harvesters yields improved power output for tailored values of coupling coefficients. The second set of results show that Lévy flight excitation fundamentally alters the bifurcation characteristics of the dynamics. Together, the results underscore the importance of non-Brownian excitation characterised by Lévy flight in vibration energy harvesting, both from a theoretical viewpoint and from the perspective of practical applications.

1 Introduction

Vibrationenergy harvesting (VEH) continues to be a topic of intense research as a promising pathway in the quest for inexpensive and sustainable sources of energy. VEH seeks to efficiently harness the energy associated with sources of ambient - and characteristically random - vibrations by converting it to electrical power. Piezoelectric transduction is a typical method of conversion of mechanical energy to electrical energy in energy harvesters. There exists an extensive body of literature on VEH, starting with attempts to autonomously power mobile sensor networks [29, 20, 24, 27, 28, 23, 4] and more recent reviews may be found in, e.g., [16, 13].

Given the objectives of this article, certain analytical aspects of VEH merit consideration next. A vibration energy harvester, in essence, is an electromechanical system. The dynamics of the harvester may be approximated by a system of ordinary differential equations that represent the coupling between the mechanical and electrical degrees of freedom. Two aspects of the dynamics that are important from both the theoretical and applied viewpoints are nonlinearity and stochasticity, and we now briefly discuss them in sequence, with a view towards motivating the research reported in this article.

Designing an efficient harvester in the linear regime of the dynamics is fundamentally challenging because maximal power output in this case is constrained on the system being consistently excited at its resonant frequency. Indeed, ambient vibrations cannot be expected to satisfy this constraint and hence attention has turned to the nonlinear regime where, in principle, better power output may be expected over a broad band of excitation frequencies [6, 2, 22, 26, 25]. Whilst under certain conditions nonlinear harvesting seems to offer better prospects (e.g. bistable oscillators [30, 21, 17]), the topic continues to be the subject of active research. However, we note that designing a nonlinear harvester is fraught with a set of unique challenges.

Turning now to stochasticity, we note that due to the random nature of ambient excitation, it is essential to consider the harvester as a stochastic dynamic system [9, 8, 12]. Consequently, nonlinear harvesters where the dynamics of the mechanical degree of freedom occurs under monostable and bistable quartic potentials of the Duffing type have been extensively studied under random excitation (see, e.g., [9, 6]). Notably, the literature on nonlinear harvesting is largely focused on the equilibrium state that the harvester is assumed to have attained under excitation characterised by Brownian (diffusive) processes and their slight variations. However, given that a harvesting device is quite unlikely to settle into a genuine steady state in practice and that the transient states likely yield higher expectation values of power output, the nonequilibrium states of the harvester dynamics need to be well understood. This serves as one of the motivating factors for the present work.

Moreover, harvester dynamics under non-Brownian excitation is yet to receive the attention it deserves. For, in addition to dynamics driven by such excitation being of intrinsic interest from a mathematical standpoint, non-Brownian processes (e.g. Lévy flights) are better suited to model excitation in several real-world harvesting scenarios such as VEH from ocean waves. Furthermore, optimised harvester circuit design that significantly enhances harvesting efficiency (see, for instance, [19]) could also benefit from a harvester driven by Lévy flight excitation. Finally, stochastic excitation characterised by non-Brownian processes can significantly influence the hysteresis phenomenon and therefore jump bifurcations in certain nonlinear harvesters. Once again, in addition to being of deep mathematical interest, jump bifurcations impact practical harvester design since they dictate the stability characteristics of operating regimes. And yet, to the best of the authors' knowledge, the dynamics and the efficiency of a piezoelectric energy harvester under Lévy flight excitation have not been studied in any detail in the literature. The only discussion one finds is in [7] where certain interesting aspects of the dynamics of a harvester undergoing motion under a Woods–Saxon potential and coloured noise of the Lévy type are reported. Indeed, all of the aforementioned considerations strongly motivate the work reported in this article.

To summarise the key objectives of this article, first we seek to understand the influence of Lévy excitation on the averaged power output from a generic piezoelectric harvester and the sensitivity of the power output to noise intensity. Since the interplay between randomness

and nonlinearity is known to engender phenomena such as stochastic resonance with potential benefits for harvesting [10], we focus on a nonlinear harvester where the mechanical degree of freedom is represented by a Duffing oscillator where we consider the two distinct cases of the quartic potential: the monostable (hardening stiffness) and the bistable (softening stiffness). In addition, harvesting using a (linearly) coupled array of Duffing oscillators is also investigated. Second, we seek to understand the influence of Brownian and Lévy excitations on the hysteresis phenomenon and jump bifurcations that arise in a nonlinear harvester with softening stiffness. In all the cases, we also seek results from Brownian excitation in order to compare and contrast the results with those obtained for Lévy excitation.

The rest of the article is set as follows. In Section 2 we present a generic analytical model of a piezoelectric energy harvester followed by a discussion of the key characteristics of Lévy flights. An outline of the numerical simulation scheme and allied details are also provided in this section. In Section 3, we present results from the linear and nonlinear cases (both monostable and bistable) both for Brownian and Lévy excitations. The results for harvested power from a coupled array are also presented in this section. In Section 4, results that illustrate the influence of Brownian and Lévy excitations and the noise intensity of the excitation on the hysteresis phenomenon are presented. The article concludes in Section 5 with a further discussion of the results and a view towards potential directions for future work.

2 Methodology

2.1 Analytical framework

The dynamics of a piezoelectric energy harvester's electrical and mechanical degrees of freedom are modelled using a system of coupled differential equations. Much work regarding such models exists in the literature. For the purposes of this article, we adopt the model described in [9]. This model is included as equations (2.1) and (2.2). The mechanical degree of freedom is represented in equation (2.1), while the electrical degree of freedom is represented in equation (2.2). These equations are coupled with one another via the constant coupling coefficients K_v and K_c. Note that these modelling equations are in fact nondimensional:

$$\ddot{x} = -\frac{dU(x)}{dx} - \gamma\dot{x} - K_v V + \sigma\xi(t), \tag{2.1}$$

$$\dot{V} = K_c\dot{x} - \frac{1}{\tau_p}V. \tag{2.2}$$

In these equations, x represents the displacement, and V the voltage. The coefficient γ is the viscous damping coefficient and τ_p is the time constant of the piezoelectric dynamics. K_v is the coupling coefficient relating the displacement to the voltage, and K_c is the piezoelectric coupling constant. The nondimensional values used for these coefficients and model parameters are identical to those referenced in [9] and [5] ($\tau_p = 11.4$, $\gamma = 0.016$, $K_c = 0.5$, $K_v = 0.5$). The $\sigma\xi(t)$ term is the stochastic process driving the harvester, where σ is a constant representing the noise intensity. $U(x)$ is the potential energy function, which in the nonlinear case corresponding to a Duffing oscillator is represented by equation (2.3). When both the constant coefficients a and b are positive, the nonlinear potential is said to be monostable. The potential becomes bistable when a is negative and b is positive. This results in a $U(x)$ function with two potential wells, the

precise shape of which is manipulated by varying a and b. We also note that when b is set to zero in equation (2.3), one recovers the potential energy for a linear oscillator:

$$U(x) = \frac{1}{2}ax^2 + \frac{1}{4}bx^4. \tag{2.3}$$

Additionally we consider in this article an array of five nonlinear harvesters that are linearly coupled to their nearest neighbours. The modelling equations for member i of such an array are included as equations (2.4) and (2.5). In equation (2.4), k_{cpl} is the coupling stiffness:

$$\ddot{x}_i = -\frac{dU(x_i)}{dx_i} - \gamma\dot{x}_i - k_{cpl}(2x_i - x_{i+1} - x_{i-1}) - K_{v_i}V_i + \sigma\xi(t), \tag{2.4}$$

$$\dot{V}_i = K_c\dot{x}_i - \frac{1}{\tau_p}V_i. \tag{2.5}$$

2.2 Stochastic excitation

The $\sigma\xi(t)$ term in the equations of the model represents the stochastic forcing where σ is the noise intensity. In the case of Brownian motion (process), $\xi(t)$ is a white noise process that generates the Brownian motion. Mathematically, $\xi(t)dt = dW$, where dW is a Weiner process. Formally, equations (2.1) and (2.2) may be rewritten as a first-order system of Ito stochastic differential equations as (see, for instance [11]):

$$d\bar{x} = \bar{A}dt + \sigma d\bar{W}, \tag{2.6}$$

where $\bar{x}$ is the state vector of the harvester given in terms of the displacement, velocity and voltage by $\bar{x} = [x, \dot{x}, V]^T$. The incremental Weiner process $d\bar{W}$ and $\bar{A}$ are defined under the change of variables $x_1 = x$, $x_2 = \dot{x}$ and $x_3 = V$ as follows:

$$\bar{A} = \begin{bmatrix} x_2 \\ -\dfrac{dU(x_1)}{dx_1} - \gamma x_2 - K_v x_3 \\ K_c x_2 - \dfrac{1}{\tau_p}x_3 \end{bmatrix}, \tag{2.7}$$

$$d\bar{W} = \begin{bmatrix} 0 \\ dW \\ 0 \end{bmatrix}. \tag{2.8}$$

The realisations of a Brownian process are random variables that are (randomly) distributed according to the standard normal distribution (please see the standard normal distribution shown in Figure 1). The distribution peaks at the origin, is symmetric about the y-axis and tapers off quickly as one moves away from the origin along the x-axis. In other words, most of the random values that are realised in a Brownian process are values close to the mean value of the distribution at the origin. In contrast to this situation is the case of a generalisation of the Brownian process called Lévy process which is characterised by a scale factor $\delta > 0$ and a shift parameter μ. The contrast with the standard normal distribution is illustrated in Figure 1 where the
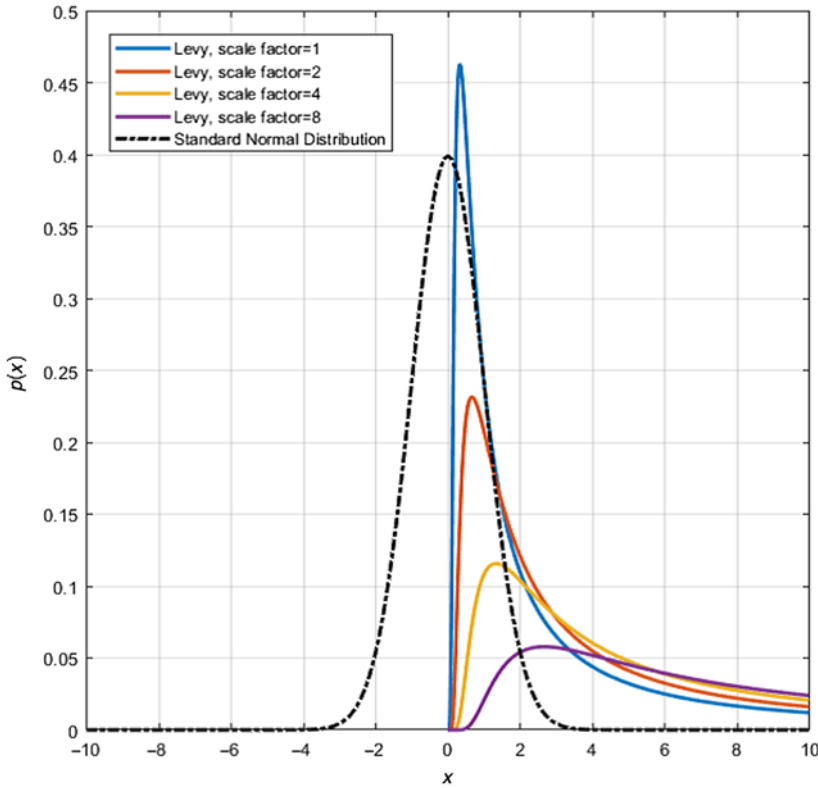
FIGURE 1. Levy and Gaussian distributions.

Lévy distribution is shown for different values of the scale factor (which determines the width of the distribution) and the shift parameter (which determines the location of the peak). As seen from the figure, depending on the scale and shift factors, the Levy distribution is long tailed; there can be a significant area under the distribution along the positive x-axis. Now, Brownian processes represent random motion about a mean where the steps are drawn from a standard normal distribution. However, as described above, Lévy processes are characterised by a long-tailed distribution. Therefore, in random motion of the harvester driven by Lévy processes, occasional motion with steps that deviate significantly from the mean can and do occur. Formally, Lévy flights are classified as a special class of continuous time random walk processes. We now present the expression for the Lévy distribution in one variable x in terms of the parameters δ and μ (see, for instance, [15]):

$$L(x, \delta, \mu) = \begin{cases} \sqrt{\dfrac{\delta}{2\pi}} \dfrac{1}{(x-\mu)^{3/2}} e^{\left(-\frac{\delta}{2(x-\mu)}\right)}; & 0 < \mu < s < \infty \\ 0; & s \leq 0. \end{cases} \tag{2.9}$$

Random excitation of the harvester in the Lévy case is considered using a bi-variate probability distribution function $\Psi(x, t) = \Lambda(x)w(t)$, where $\Lambda(x)$ is called the jump-length distribution and $w(t)$ is called the wait-time distribution [15]. The wait-time distribution corresponds to an uncorrelated (Markovian) process, while the jump distribution is Lévy. We note here that a

convenient way to represent a Lévy distribution, say $f(x)$, is via its Fourier transform $F(k)$ which always has the form [1]:

$$F(k) = \exp(-\lambda|k|^{\alpha}); \ 0 < \alpha \leq 2, \tag{2.10}$$

where the constant $\lambda(-1 \leq \lambda \leq 1)$ indicates the skewness of the distribution and the constant α, called the Lévy index, dictates the area under the tail region of the distribution.

Modifying the harvester model for the case of Lévy excitation entails replacing the Weiner process dW by the Lévy increment dL_t^{α}, where α is the Lévy index of the distribution. For this article, we consider $\alpha = 1.4$. As in the Brownian case, this increment is multiplied by the constant σ, which represents the noise intensity.

2.3 Numerical scheme

Numerical simulations are accomplished using the well-known Euler–Maruyama numerical method for stochastic systems [14]. A duration of 200 s and a time step rate of 1000 Hz are used. Generating noise, both Brownian and Lévy, is accomplished via methods available in literature ([31] and [14], respectively). The numerical implementation of the Lévy increments is slightly more involved than for the Brownian case. This task is handled by using a method known as Mantegna's algorithm (see [31]).

The energy output E is calculated from the power output P using the relationship $E = \int P(t)\,dt$. In the discrete case (as in the simulations), the integral is replaced by a summation. For a time interval $[a, b]$ split into $N + 1$ evenly spaced points, the integral of a function $f(t)$ would be replaced by a summation as follows:

$$\int_a^b f(t)dt \approx \frac{b-a}{2N} \sum_{n=1}^{N} \left(f(t_n) + f(t_{n+1}) \right) \tag{2.11}$$

$$= \frac{b-a}{2N} \left[f(t_1) + 2f(t_2) + ... + 2f(t_N) + f(t_{N+1}) \right], \tag{2.12}$$

where $(b - a)/(2N)$ is the spacing between each point, which in this case is equal to the numerical step size dt.

3 Results: harvested power

As stated earlier, the objective of our effort is to compare the power output from the harvester between Brownian and Lévy excitations in a variety of cases. In each case, the power output is calculated as follows. First, the instantaneous power is calculated from the output voltage of the harvester at each time step of the simulation by considering a load resistance of $1M\Omega$ and using the standard formula, Power $= V^2/R$ where V is the voltage and R is the resistance. Second, in order to obtain reliable results, 50 unique simulations are conducted for each case and the root-mean-squared (RMS) value of the power output at each time step across all 50 simulations is computed. This is the power output plotted in the graphs for all the cases. We also note that a distinct noise profile (depending on whether the noise in Brownian or Lévy) is consistently used for each of the 50 simulations (i.e. 50 distinct noise profiles for Brownian and 50 distinct noise profiles for Lévy) in order to obtain reliable averaged values of power output. Finally, we note

(a)

(b)
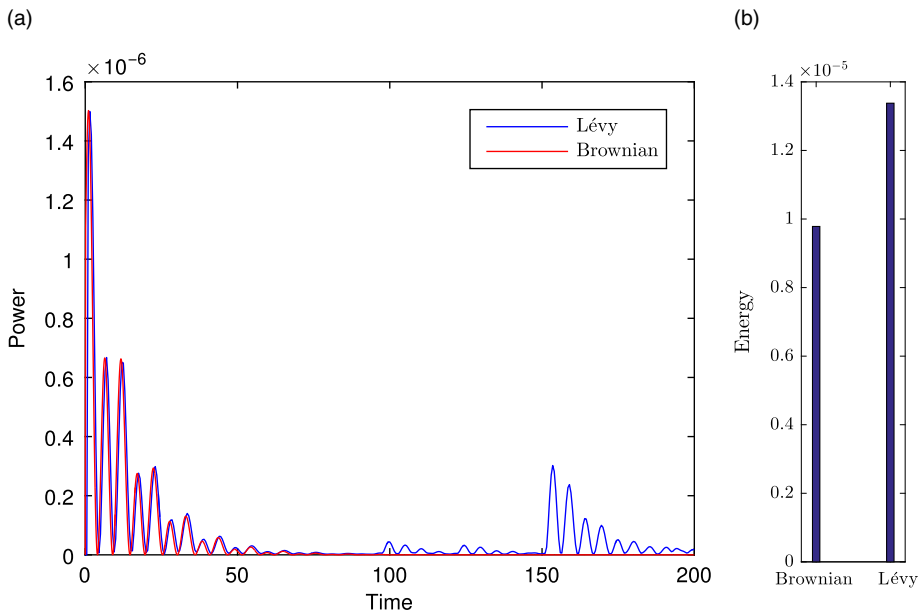
FIGURE 2. Linear harvester: noise intensity $\sigma = 0.0012$ (a) RMS power output (b) total energy output.

that the energy output shown in the bar graphs for each case is obtained by integrating the power output with respect to the time step for the entire duration of each simulation. Both the power and energy shown are nondimensional. In this section we present results for the cases of the linear harvester, monostable harvester, coupled harvester array and the bistable harvester.

3.1 Linear harvester

The averaged power output, for both Lévy and Brownian noise of identical intensity $\sigma = 0.0012$, is presented in Figure 2(a). This result demonstrates that while the power outputs due to Lévy and Brownian noise are almost identical during early times of the simulation, over the full-time duration Lévy noise excitation leads to a higher amount of power harvested. This is due to the higher energy of excitation caused by the occasional large deviations from the mean in the Lévy noise case. It is of interest to note that the harvester is able to convert a portion of the disordered energy associated with noise into electrical power. The higher energy output in the Lévy excitation case is further established quantitatively by the comparison bar graphs presented in Figure 2(b).

For the previous simulations, the noise intensity was held constant at $\sigma = 0.0012$. To better understand the influence of varying the noise intensity on the power output in both the Lévy and Brownian cases, a parametric study is conducted next. Power output is compared for five different σ values. Each σ value is treated to the same 50 noise profiles to ensure accurate comparisons. RMS power output results for the linear harvester excited by Lévy noise are included in Figure 3(a). As expected, increasing the noise intensity results in higher RMS power output levels. This is not surprising as higher noise intensity directly translates to more energy being input into the system. The corresponding higher energy output is observed from Figure 3(b) as well.

(a)

(b)
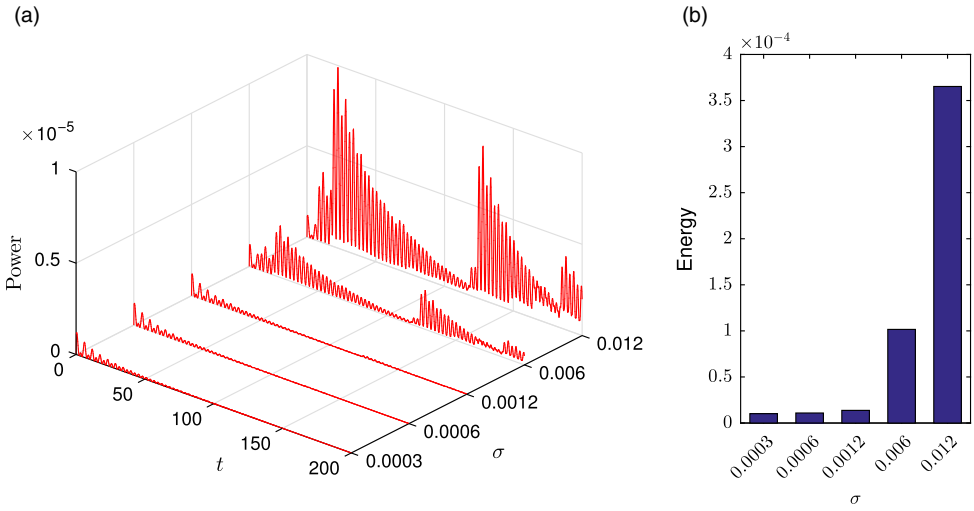
FIGURE 3. Linear harvester: Lévy noise, multiple σ values (a) RMS power output (b) total energy output.

(a)

(b)
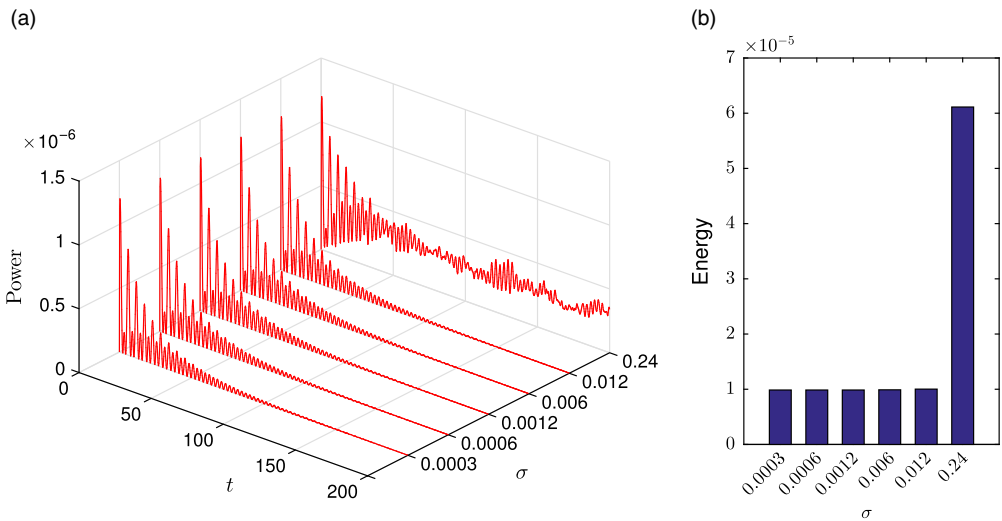
FIGURE 4. Linear harvester: Brownian noise, multiple σ values (a) RMS power output (b) total energy output.

To better understand the significance of the results obtained by varying the noise intensity in the Lévy case, we repeat the analysis using Brownian noise. The results for the RMS power output are presented in Figure 4(a), and the energy output results in Figure 4(b). Immediately a stark contrast can be seen between the results for the Brownian case and the Lévy case. When varying the noise intensity within the range considered in the Lévy case, the output for the Brownian case is unchanged. Only when σ is increased further to say, 0.24 as in the figure, do we notice a change. This higher noise leaves the peak power output essentially unchanged, but induces some instability in the system response. This is a noteworthy contrast to the Lévy case, where smaller
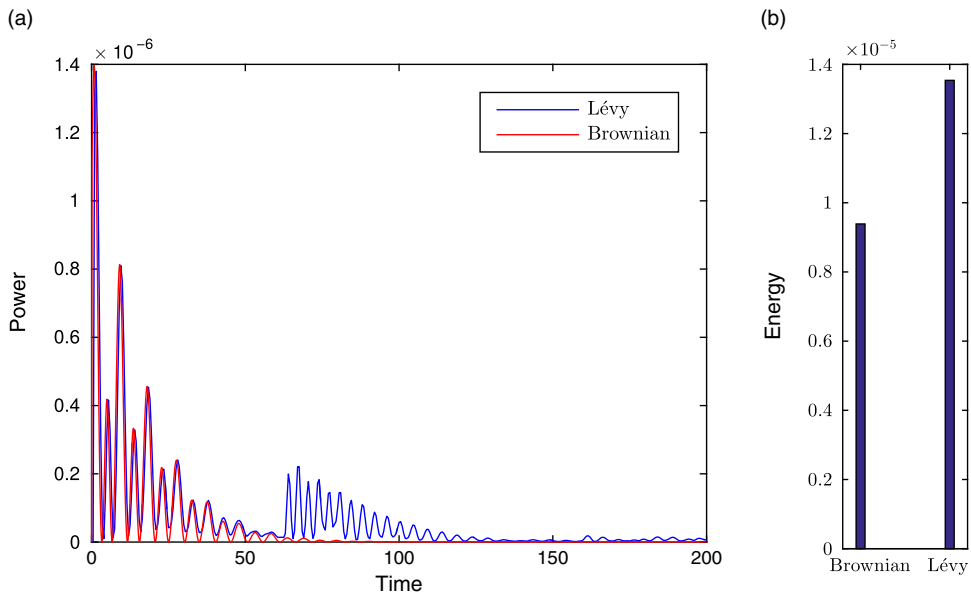
FIGURE 5. Nonlinear harvester: monostable case, $\sigma = 0.0012$ (a) RMS power output (b) total energy output.

changes in σ brought large increases in peak power delivery. As such it can be concluded that the linear harvester is more sensitive to variations in noise intensity when the noise is of the Lévy type. This is a key result of this article and, as will be seen in the results that follow, this holds for the nonlinear case as well.

3.2 Nonlinear harvester: monostable potential

With baseline linear results established, our attention turns to a harvester with a nonlinear, monostable potential, as shown in equation (2.3). For these simulations, values for a and b are adopted from [9], and in this case are $a = 0.1$ and $b = 0.1$. The same RMS averaging scheme used for the linear case is employed here, with the same load resistance used in calculating power and the noise intensity maintained at $\sigma = 0.0012$. The results for this monostable nonlinear harvester under both noise types are provided with the RMS power output in Figure 5(a) and the energy output in Figure 5(b). Lévy flight has here once again proven more fruitful, producing higher power outputs than the Brownian case.

As in the linear case, one would now seek to understand the effects of varying the noise intensity σ on the harvested power. Once again, the same 50 run RMS averaging scheme is employed and simulations are carried out with respect to five different σ values. Each σ value is treated to the same 50 noise profiles to ensure accurate comparisons. The results for the monostable nonlinear harvester with $a = 0.1$ and $b = 0.1$ as before but now for different σ values under Lévy excitation are included in Figure 6. The conclusions here are similar to the linear case, as increasing the noise intensity increased the levels of power harvested.

We now repeat the parametric analysis by varying σ using Brownian noise. The results for nonlinear monostable harvester are presented in Figure 7. The contrast observed in the results

(a)

(b)
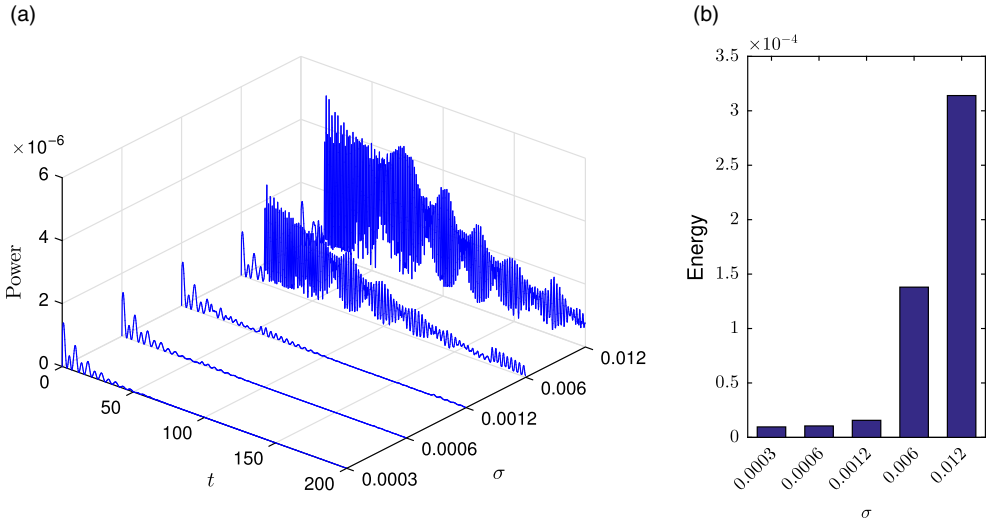
FIGURE 6. Nonlinear monostable, Lévy noise, multiple σ (a) RMS power output (b) total energy output.

(a)

(b)
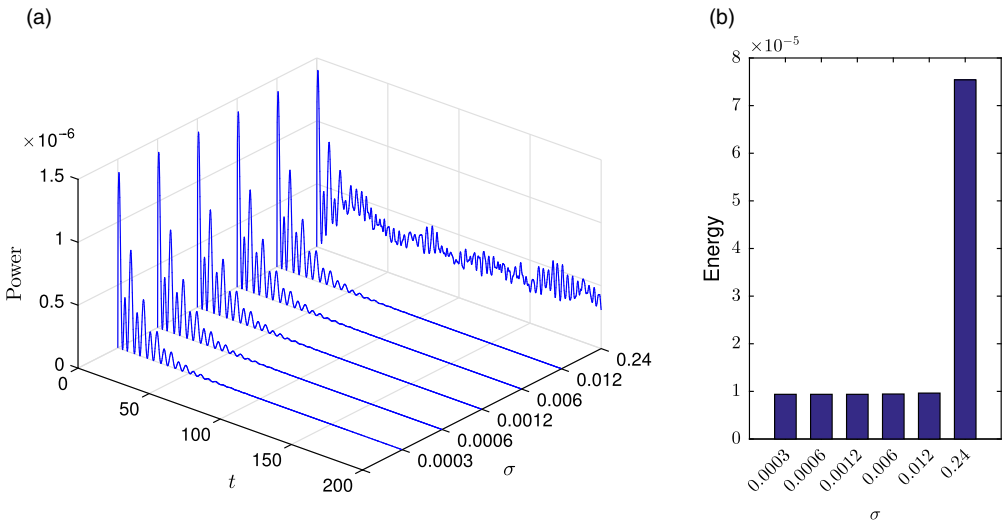
FIGURE 7. Nonlinear monostable, Brownian noise, multiple σ (a) RMS power output
(b) total energy output.

for the Brownian noise and the Lévy noise for the linear harvester case is evident here as well. When varying the noise intensity within the range considered in the Lévy case, the output for the Brownian case remains essentially unchanged. Only when σ is further increase to say, 0.24, do we notice a change. This higher noise leaves the peak power output essentially unchanged as well, but induces some instability in the system response. However, for the Lévy case, smaller changes in σ resulted in large increases in peak power delivery. Hence, one of the key results of this article that the harvester is more sensitive to variations in noise intensity when the noise is of the Lévy type is valid for the nonlinear monostable case considered as well.
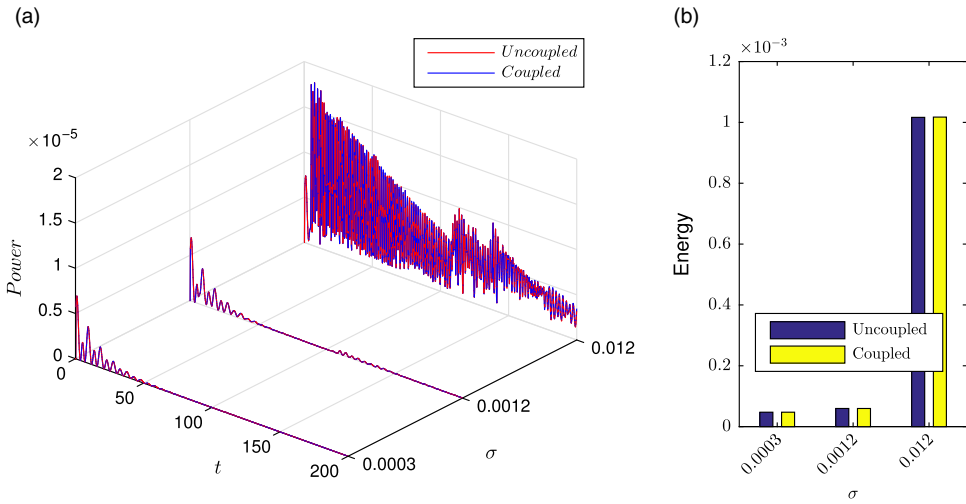
FIGURE 8. Lévy noise, coupled vs. uncoupled, $k_{cpl} = 0.01$ (a) RMS power output (b) total energy output.
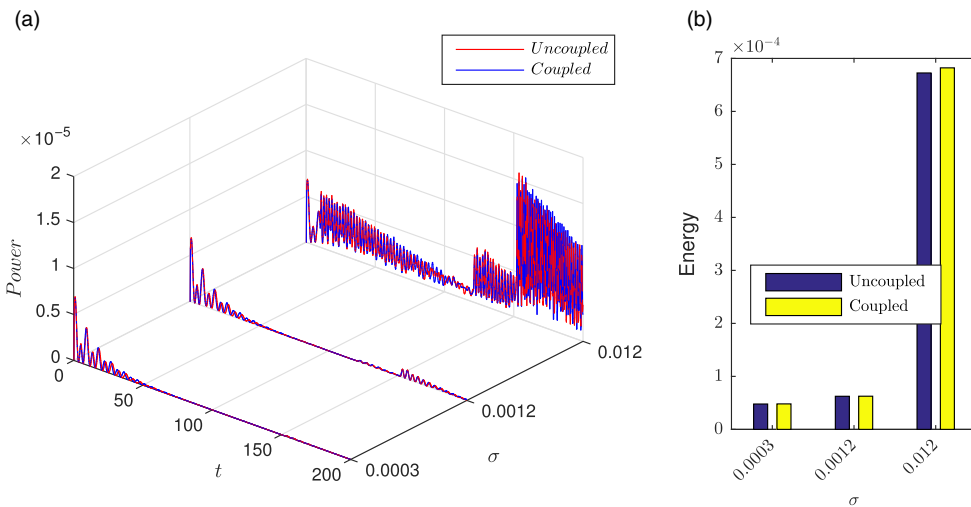
FIGURE 9. Lévy noise, coupled vs. uncoupled, $k_{cpl} = 0.1$ (a) RMS power output (b) total energy output.

3.3 Coupled harvester array

Next we turn our attention to an array of harvesters physically coupled to their nearest neighbours since a coupled configuration is of interest in practical applications. Of particular interest is the influence of the magnitude of the coupling stiffness k_{cpl} on the harvested power. The parameter k_{cpl} dictates the strength of the coupling between the individual harvesters in the array. The equations for the array are, as described before, equations (2.4) and (2.5). The array considered here consists of five nonlinear harvesters linearly coupled to their nearest neighbours. Each harvester is subject identical excitation. Simulations are run simultaneously for five uncoupled harvesters to serve as a benchmark. The results for the two systems under Lévy noise in Figures 8–10 reveal

(a)

(b)
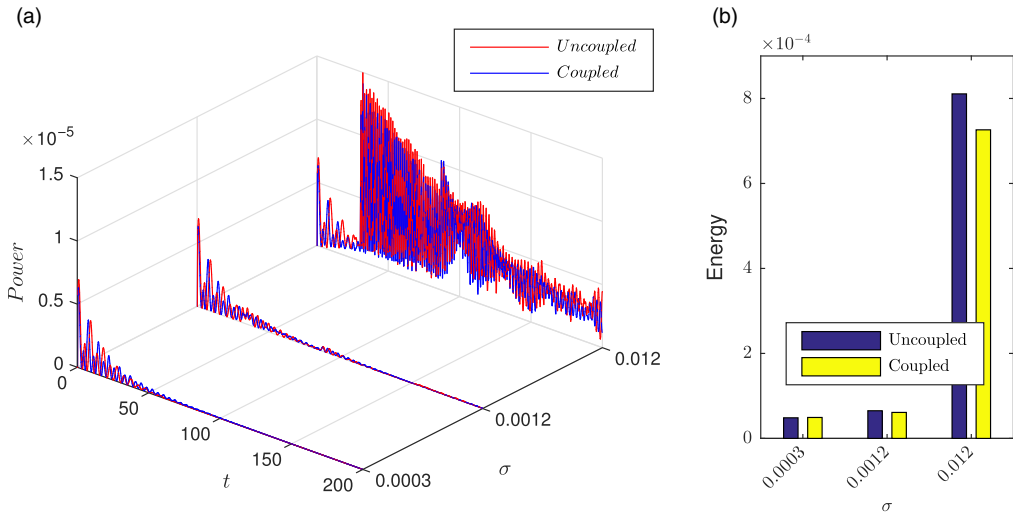
FIGURE 10. Lévy noise, coupled vs. uncoupled, $k_{cpl} = 1.0$ (a) RMS power output (b) total energy output.

that the output is indeed sensitive to the coupling stiffness (k_{cpl}). For the lowest value $k_{cpl} = 0.01$, i.e. weakest coupling amongst all the cases considered, the results for which are in Figure 8, we see that the output for the coupled array is essentially comparable to that of the uncoupled array. Figure 9 demonstrates that increasing the coupling stiffness to $k_{cpl} = 0.1$ results in the coupled array outperforming its uncoupled counterpart, but only slightly. This is a key result as it demonstrates that coupling can improve energy harvesting when properly implemented. The benefit of increasing k_{cpl} does not endure however, as increasing it to $k_{cpl} = 1.0$, as in Figure 10, results in the uncoupled system performing the best.

To put these coupling results for Lévy noise in better context, we carry out the same exercise for Brownian noise. The results for the same three k_{cpl} values are included in Figures 11–13. For the two lowest values, $k_{cpl} = 0.01$ and $k_{cpl} = 0.1$, we see that the output is essentially the same for both the coupled and uncoupled systems. Increasing k_{cpl} to 1.0 results in the coupled system performing best. This contrasts the Lévy case where $k_{cpl} = 1.0$ favoured the uncoupled system. The benefit of coupling under Brownian noise with $k_{cpl} = 1.0$ is more apparent than any benefit seen with any k_{cpl} values when Lévy noise is considered. This suggests coupling is a more beneficial addition when the system is subject to Brownian noise and not Lévy noise.

3.4 Nonlinear harvester: bistable potential

The final set of results reported in this section are those for the case of a bistable potential with distinct parameter values. As mentioned in the Introduction, we are motivated by the literature that reports on the advantages of bistable harvesters (see, for instance, [30, 21, 17]). We reiterate that bistability is represented by the stiffness constant "a" in equation (2.3) being negative, while the constant "b" positive. First the magnitudes of a and b are taken as equal to those used in earlier simulations ($|a| = 0.1$, $|b| = 0.1$). The results for Lévy noise are included in Figure 14. In this figure, importantly, the gain in harvested energy is enhanced due to increased noise intensity for the bistable system.

(a)

(b)
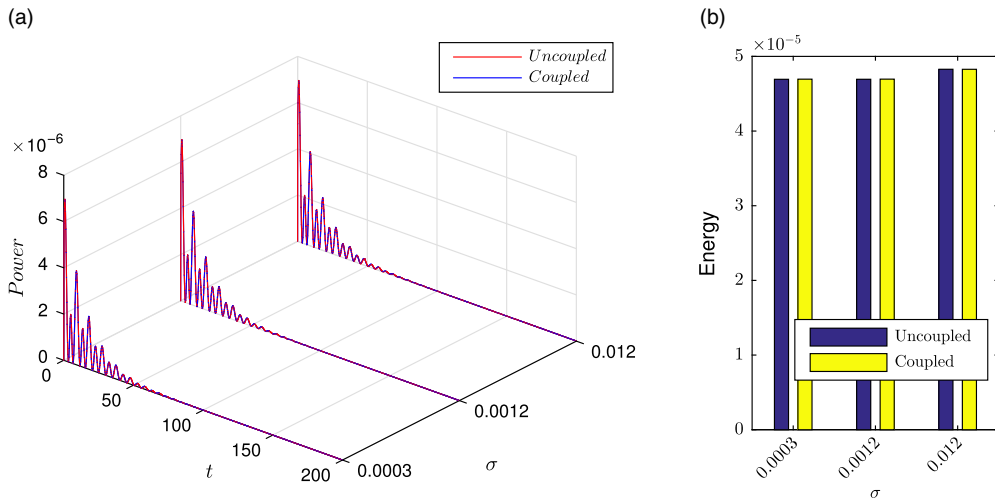
FIGURE 11. Brownian noise, coupled vs. uncoupled, $k_{cpl} = 0.01$ (a) RMS power output
(b) total energy output.

(a)

(b)
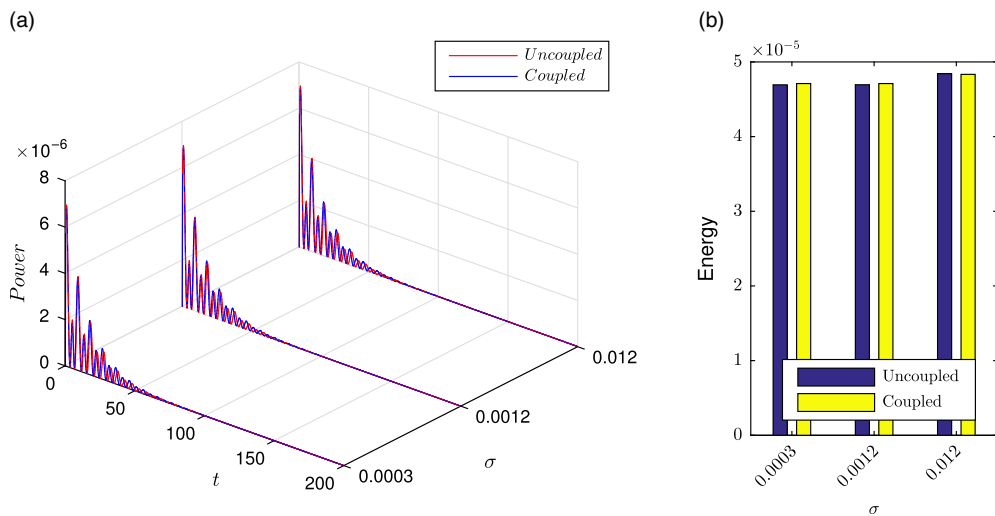
FIGURE 12. Brownian noise, coupled vs. uncoupled, $k_{cpl} = 0.1$ (a) RMS power output
(b) total energy output.

Next, in order to investigate the comparative response of a bistable harvester to Lévy and Brownian noise of varying intensity, we set $a = -0.15$ and $b = 0.01$ and consider three σ values of increasing magnitude, $\sigma = 0.0006,\ 0.012,\ 0.016$. The results for the Lévy noise case under the above parameters are included in Figure 15. The results for parameters identical as before but now subjected to Brownian noise are included in Figure 16. The key conclusions for the bistable harvester are: (1) Lévy noise leads to higher harvested power (there is an order of magnitude difference in the energy output between Brownian and Lévy) and (2) the variation considered for the noise intensity has a much more significant effect on harvester energy in the Lévy case.

(a)

(b)
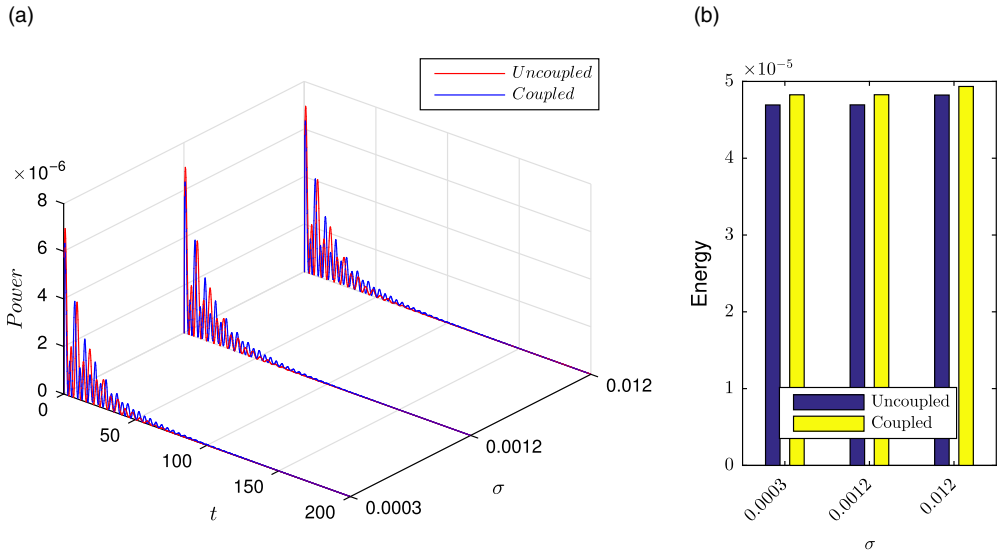
FIGURE 13. Brownian noise, coupled vs. uncoupled, $k_{cpl} = 1.0$ (a) RMS power output (b) total energy output.

(a)

(b)
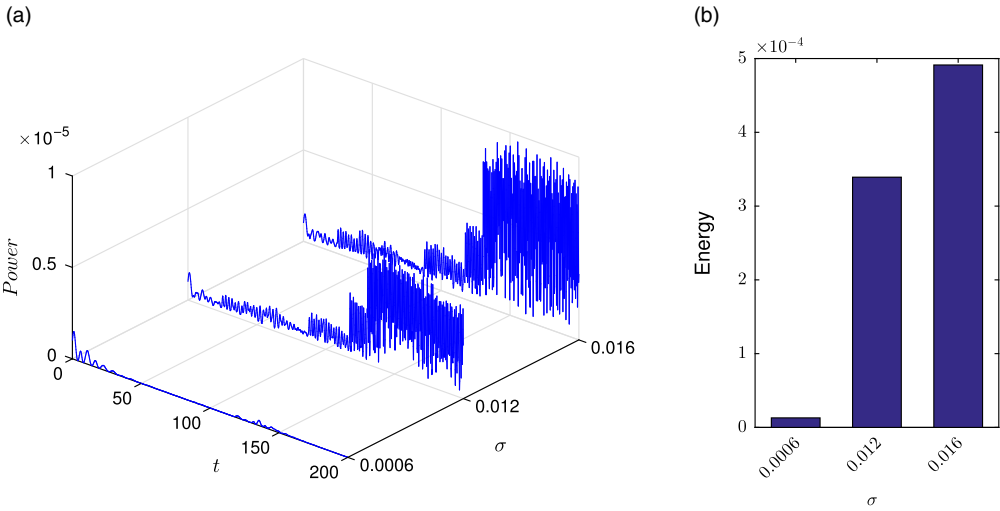
FIGURE 14. Bistable harvester: $a = -0.1$, $b = 0.1$, Lévy noise (a) RMS power output (b) total energy output.

We note from Figure 16 that the harvested energy is much less sensitive to variations of noise intensity in the Brownian case. Overall, while a direct comparison between a monostable and bistable harvester cannot be considered significant since both cases correspond to qualitatively different potential energy functions, the results show that the benefits of Lévy excitation over Brownian for harvested energy are evident in the bistable case as well.

(a)

(b)
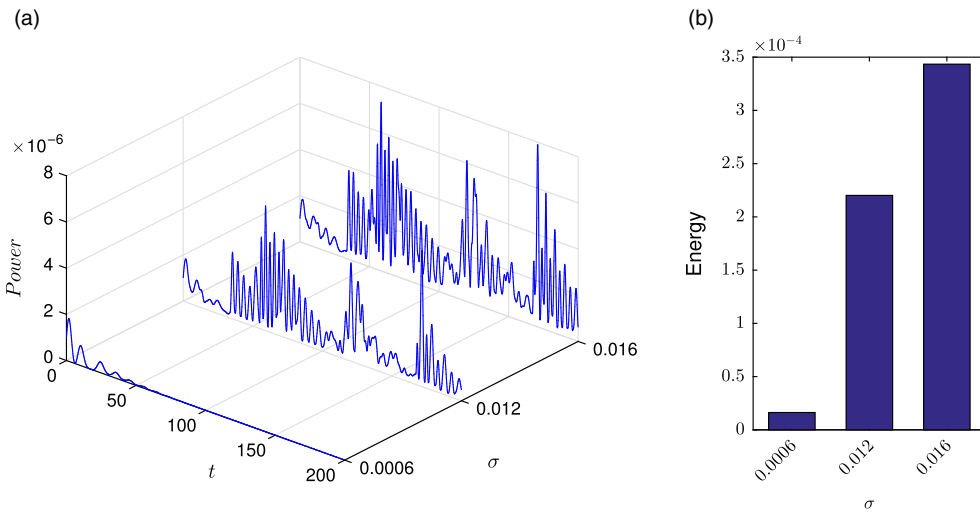
FIGURE 15. Bistable harvester: $a = -0.15$, $b = 0.01$, Lévy noise (a) RMS power output (b) total energy output.

(a)

(b)
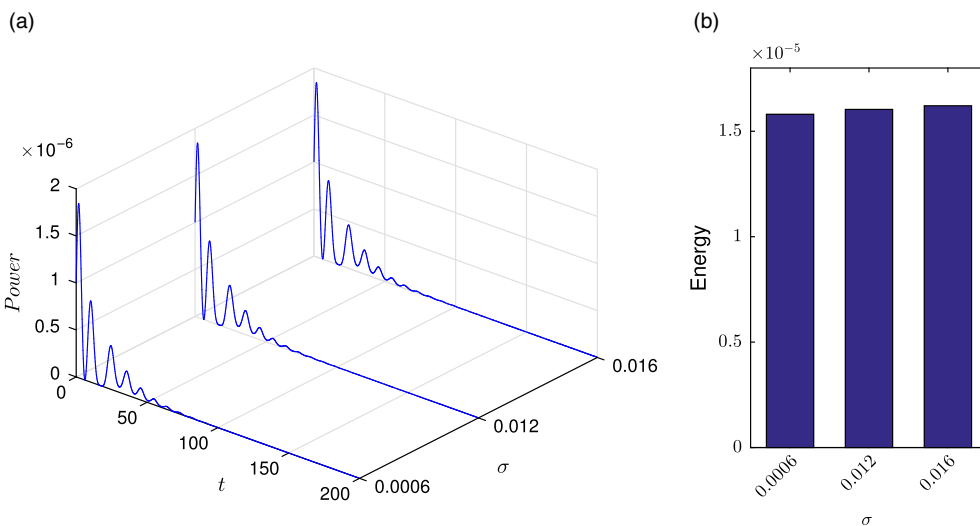
FIGURE 16. Bistable harvester: $a = -0.15$, $b = 0.01$, Brownian noise (a) RMS power output (b) total energy output.

4 Results: hysteresis and jump bifurcations

When considering a nonlinear system, noise can have interesting effects on the presence and characteristics of system bifurcations. Here we consider the effects of noise on the hysteresis phenomenon which corresponds to jump bifurcations in a harvester with softening nonlinear stiffness. In this case, the equation of motion of the mechanical degree of freedom can be reduced to that of a Duffing oscillator with softening stiffness. The basis of our analysis are the *deterministic* results on the hysteresis phenomenon and jump bifurcations in the Duffing oscillator
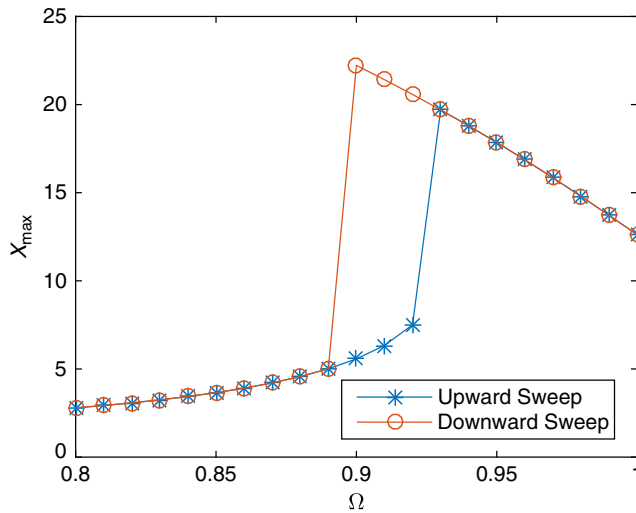
FIGURE 17. Frequency response, deterministic case: $\sigma = 0$.

reported by Brennan et al. [3]. The hysteresis phenomenon is well known in a Duffing oscillator and corresponds to jump bifurcations (see, for instance [18]). To summarise, the frequency response curve is the plot of the maximum steady state response amplitude of an oscillator (X_{max}) with respect to the frequency of external excitation (Ω). For a linear oscillator, the frequency response X_{max} is a linear function of Ω, while for a Duffing oscillator, it is a nonlinear function. In particular, X_{max} becomes a multiple-valued function of Ω resulting in a hysteresis loop as seen in Figure 17. Correspondingly, if Ω is slowly decreased (Downward Sweep), X_{max} suddenly jumps down (the red line) and if if Ω is slowly increased (Upward Sweep), X_{max} suddenly jumps up (the blue line). This phenomenon is called a jump bifurcation and the hysteresis region is a region of instability in the sense that X_{max} changes suddenly for Ω values in this region.

In this section we present results on the effect of Brownian and Lévy noise on the hysteresis loop and therefore the jump bifurcations. To the best of the authors' knowledge, this aspect has not been investigated in the literature. For these simulations, we first set the derivative of the voltage equal to zero, thus turning equation (2.2) into a linear relation between the velocity and voltage. This is used to eliminate the voltage term from equation (2.1). Damping (ψ) and stiffness (α) parameters are taken from [3] and accordingly set to $\psi = 0.04$ and $\alpha = -5.9 \times 10^{-4}$. The equation for the mechanical degree of freedom x of the harvester, now subject to excitation that is an additive combination of a harmonic excitation of amplitude unity and frequency Ω and the noise term $\sigma \xi(t)$ is then obtained as:

$$\ddot{x} = -x - \alpha x^3 - \psi \dot{x} + cos(\Omega t) + \sigma \xi(t). \tag{4.1}$$

In order to generate the hysteresis loop in the frequency response curve, the simulations involve both an up-sweep and down-sweep in frequency, with the maximum achieved steady-state displacement as the output. The frequency range used to study the hysteresis loop is based on the results in [3]. An individual simulation is performed at each frequency. When moving along the frequency spectrum, the final state variable values at one frequency become the initial conditions for the simulation at the next frequency. In order to achieve for better
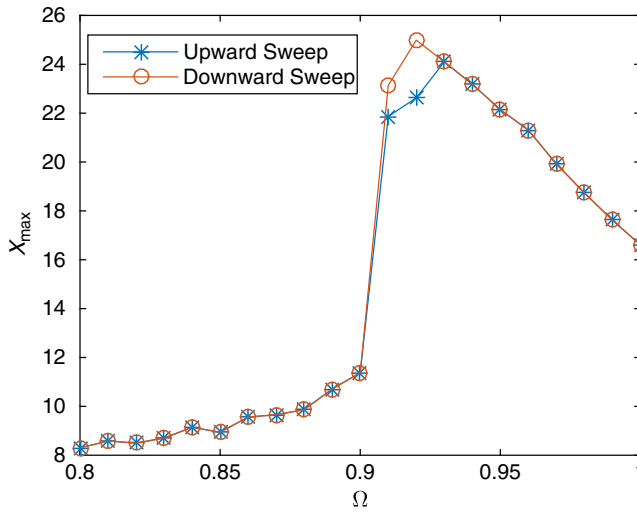
FIGURE 18. Frequency response, Brownian noise, $\sigma = 0.5$.
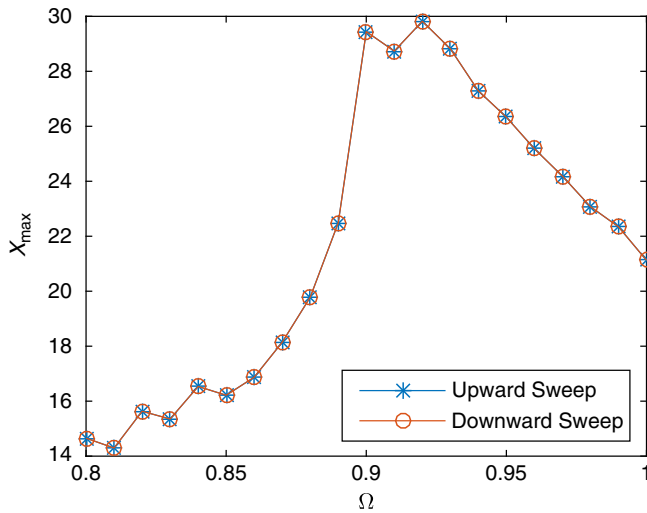
FIGURE 19. Frequency response, Brownian noise, $\sigma = 1$.

accuracy for simulations involving noise, 20 repeat simulations, each with a different noise profile, are performed at each frequency. An average of the maximum displacement values (i.e. maximum steady state values of x) across these simulations is then taken and plotted as X_{max}.

To establish a baseline understanding of how noise might affect the hysteresis loop, we begin our analysis with Brownian noise. These results are included in Figures 17–19. The results in Figure 17 represent the case where there is no noise. In this figure, the hysteresis loop formed by the results of the up-sweep and down-sweep is clearly present. In Figure 18, where $\sigma = 0.5$, we see that increasing the noise intensity acts to essentially close the gap between the data points for the up- and down-sweep, i.e. shrink the hysteresis loop. With $\sigma = 1$, in Figure 19, we see
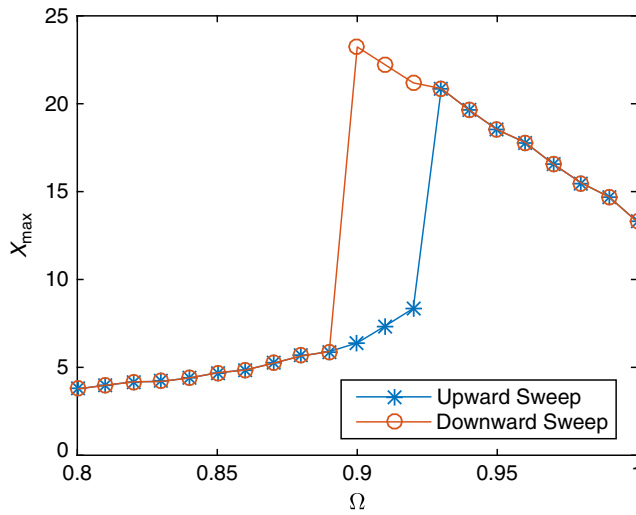
FIGURE 20. Frequency response, Lévy noise, $\sigma = 0.003$.
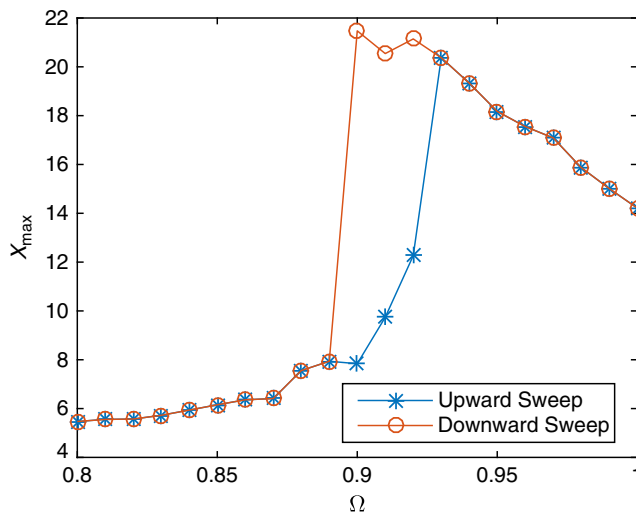
FIGURE 21. Frequency response, Lévy noise, $\sigma = 0.007$.

the gap has been closed completely and the hysteresis loop has vanished. Consequently, it can be concluded that Brownian noise of appropriate intensity can eliminate the hysteresis loop and hence the jump bifurcation phenomenon in the harvester considered.

Moving to Lévy noise, we notice slightly more temperamental behaviour. With this noise type, the system is once again much more sensitive to changes in the noise intensity. For very low σ values, as seen in Figure 20 with $\sigma = 0.003$, we clearly see the existence of the hysteresis loop. However, if we increase the noise intensity to $\sigma = 0.007$ as in Figure 21, we notice that some of the upward sweep values within the hysteresis loop are starting to approach their down-sweep counterparts thus shrinking the area inside the loop.
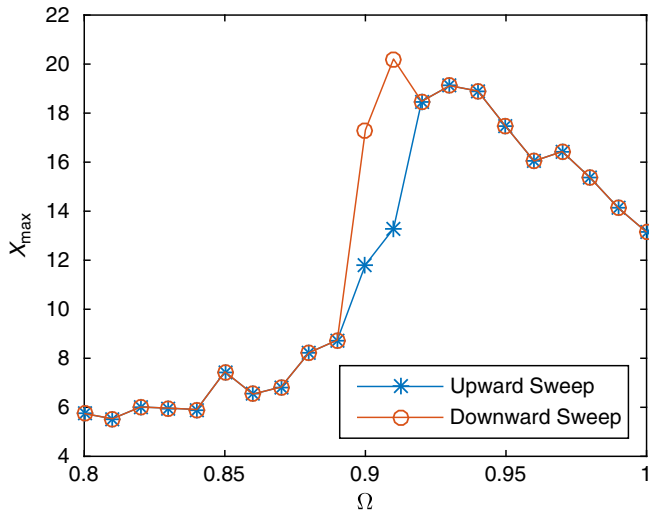
FIGURE 22. Frequency response, Lévy noise, $\sigma = 0.011$.
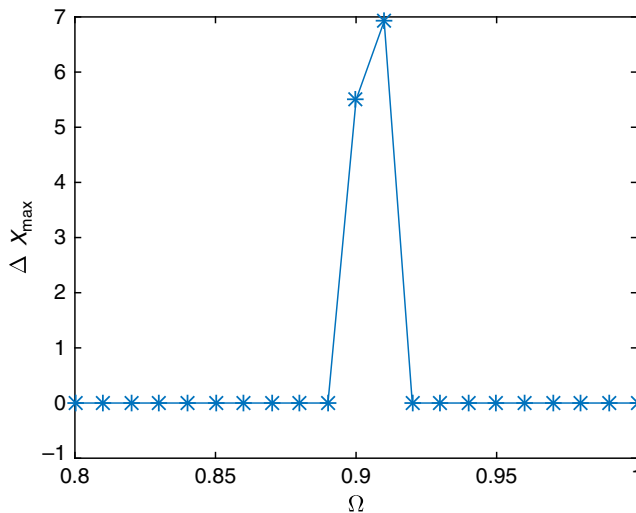
FIGURE 23. Difference between up-sweep and down-sweep data points, Lévy noise, $\sigma = 0.011$.

The loop begins to close further when the noise intensity continues to rise. This is especially clear in Figure 22, where $\sigma = 0.011$ and the discrepancies between frequency points in the loop area are clearly less. To quantify this, the differences between the up-sweep and down-sweep data points (we call it ΔX_{max}) for the $\sigma = 0.011$ case are plotted as a function of frequency in Figure 23. The difference between these points is zero for most frequencies except two points around $\Omega = 0.9$. It can therefore be concluded that Lévy noise, like Brownian noise, closes the bifurcation gap, except for some frequencies near the resonant peak.

However, there are some caveats to this conclusion. In Figure 24, where $\sigma = 0.009$, we see there is a down-ward sweep frequency point missing. This missing point indicates that the
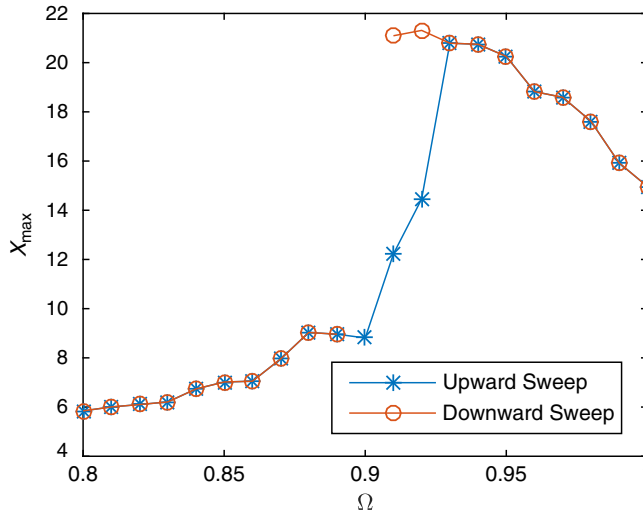
FIGURE 24. Frequency response, Lévy noise, $\sigma = 0.009$.

maximum displacement amplitude at that frequency becomes unbounded. Thus Lévy noise shrinks the hysteresis loop in a fashion similar to that seen with Brownian noise, except for some sporadic cases of instability. It should also be noted that when σ values approach 0.011, we noticed that some simulation attempts are unstable and fail completely. This confirms that the effects of Lévy noise on the hysteresis loop and hence the jump bifurcations are more erratic than those due to Brownian noise. This conclusion has important implications as it shows that when a system is excited by noise that is closer in behaviour to Lévy noise than Brownian noise, a previously predictable frequency response may be drastically altered.

5 Conclusions

In this article we have considered the effect of Lévy flight excitation on the dynamics of several different piezoelectric harvester designs and their associated average power outputs. Different designs included linear, nonlinear monostable, nonlinear bistable potentials for the mechanical degree of freedom of the harvester as well as coupled harvester systems. Simulating the dynamics was accomplished using a numerical scheme and a set of stochastic differential equations representing the dynamics of the harvester. Multiple runs were performed, and the average power output across these runs was taken at each point in time.

The first set of results demonstrate that, on average, harvesters under Lévy excitation will yield more power than those subjected to Brownian excitation. Additionally, increasing the noise intensity results in different behaviour depending on which type of noise is present. For Lévy noise, the harvester is much more sensitive to changes in the noise intensity than when subjected to Brownian excitation. This is an important conclusion of this article. When comparing a system of five harvesters coupled to together to an uncoupled counterpart, coupling was found beneficial regardless of noise type. Lastly, the benefits of Lévy excitation over Brownian were also found in an appropriately designed nonlinear bistable harvester.

The second set of results indicate that both Brownian and Lévy excitation can fundamentally alter the jump bifurcation phenomenon in the harvester. Precisely, the hysteresis loop gets eliminated for certain levels of noise intensity thereby fundamentally altering the frequency response. Moreover, the results indicate instability for higher levels of noise intensity.

Taken together, the results provide interesting insights into harvester dynamics. We note that the efficiency of energy harvesting is enhanced by optimised power extraction methods (see, for instance, [19]), and these could be improved significantly from a harvester driven by Lévy excitation. Indeed, this leads to the question of which practical harvesting applications would benefit from design based on Lévy excitation. Energy harvesting is actively researched in a wide variety of contexts such as pedestrian traffic, automotive dynamics, wearable devices, ocean wave energy and so on. In several of these applications, the excitation would be characterised by occasional large deviations from the mean, and the results of this article motivate harvester design based on Lévy excitation in those cases. Furthermore, as nonlinear harvesters increasingly take centre stage, harvester design requires careful consideration of bifurcations in order to identify stable operating regimes, and the results presented here are expected to be useful in that context as well.

The results reported in this article also lead to several interesting questions. From an applied viewpoint, experimental validation of the results would be an important direction of further research. Indeed, this would be a prerequisite for efficient harvester design in practice. Several questions emerge from a theoretical perspective as well. For instance, it would be important and interesting to (1) obtain analytical characterisation of the fact that varying the noise intensity leads to significant increase in power output for the Lévy excitation, (2) obtain a mathematical description of how random excitations (both Brownian and Lévy) alter the jump bifurcation and further investigate stochastic stability and (3) obtain a deeper understanding of the inter-well transitions in the bistable potential induced by Lévy noise. It is well known that Lévy processes are singular in certain respects, correspond to fractional diffusion operators in the time domain and are often better tackled analytically in the Fourier domain. The authors intend to pursue some of these and allied questions in future work and conclude with the hope that the results in this article spur further research on the role of Lévy excitation in nonlinear energy harvesting.

Conflict of interest

None.

Acknowledgements

References

[1] APPLEBAUM, D. (2009) *Lévy Processes and Stochastic Calculus*, Cambridge University Press, Cambridge.

[2] BARTON, D., BURROW, S. & CLARE, L. (2010) Energy harvesting from vibrations with a nonlinear oscillator. *ASME J. Vib. Acoust.* **132**, 021009.

[3] BRENNAN, M., KOVACIC, I., CARRELLA, A. & WATERS, T. (2008) On the jump-up and jump-down frequencies of the Duffing oscillator. *J. Sound Vib.* **318**, 1250–1261.

[4] COOK-CHENNAULT, K., THAMBI, N. & SASTRY, A. (2008) Powering MEMS portable devices–review of non-regenerative and regenerative power supply systems with special emphasis on piezoelectric energy harvesting systems. *Smart Mater. Struct.* **17**, 143001.

[5] COTTONE, F., VOCCA, H. & GAMMAITONI, L. (2009) Nonlinear energy harvesting. *Phys. Rev. Lett.* **102**, 080601.

[6] DAQAQ, M., MASANA, R., ERTURK, A. & QUINN, D. (2014) Closure to "Discussion of 'On the role of nonlinearities in energy harvesting: a critical review and discussion'". *Appl. Mech. Rev.* **66**, 040801.

[7] DEZA, J., DEZA, R. & WIO, H. (2012) Wide-spectrum energy harvesting out of colored Lévy-like fluctuations, by monostable piezoelectric transducers. *EPL* **100**, 38001.

[8] GAMMAITONI, F. COTTONE, L. NERI, I. & VOCCA, H. (2009) Noise harvesting. *AIP Conf. Proc.* **1129**, 651.

[9] GAMMAITONI, L., NERI, I. & VOCCA, H. (2009) Nonlinear oscillators for vibration energy harvesting. *Appl. Phys. Lett.* **94**, 164102.

[10] GAMMAITONI, L., HÄNGGI, P., JUNG, P. & MARCHESONI, F. (1998) Stochastic resonance. *Rev. Mod. Phys.* **70**, 223.

[11] GARDINER, C. (2009) *Stochastic Methods*, Vol. **4**, Springer, Berlin.

[12] GREEN, P., WORDEN, K., ATALLA, K. & SIMS, N. (2012) The benefits of Duffing-type nonlinearities and electrical optimisation of a mono-stable energy harvester under white Gaussian excitations. *J. Sound Vib.* **331**, 4504–4517.

[13] HARNE, R. & WANG, K. (2013) A review of the recent research on vibration energy harvesting via bistable systems. *Smart Mater. Struct.* **22**, 023001.

[14] HIGHAM, D. (2001) An algorithmic introduction to numerical simulation of stochastic differential equations. *SIAM Rev.* **43**, 525–546.

[15] JANAKIRAMAN, D. & SEBASTIAN, K. (2012) Path-integral formulation for Lévy flights: evaluation of the propagator for free, linear, and harmonic potentials in the over- and underdamped limits. *Phys. Rev. E* **86**, 061105.

[16] KIM, H., KIM, J. & KIM, J. (2011) A review of piezoelectric energy harvesting based on vibration. *Int. J. Precis. Eng. Man.* **12**, 1129–1141.

[17] MASANA, R. & DAQAQ, M. (2009) Relative performance of a vibratory energy harvester in mono- and bi-stable potentials. *J. Sound Vib.* **330**, 6036–6052.

[18] NAYFEH, A. & MOOK, D. (1979) *Nonlinear Oscillations*, Wiley, New York.

[19] OTTMAN, G., HOFMANN, H. & LESIEUTRE, G. (2003) Optimized piezoelectric energy harvesting circuit using step-down converter in discontinuous conduction mode. *IEEE Trans. Power Electron.* **18**, 696–703.

[20] PARADISO, J. & STARNER, T. (2005) Energy scavenging for mobile and wireless electronics. *IEEE Pervas. Comput.* **4**, 18–27.

[21] PELLEGRINI, S., TOLOU, N., SCHENK, M. & HERDER, J. (2013) Bistable vibration energy harvesters: a review. *J. Intell. Mater. Syst. Struct.* **24**.

[22] QUINN, D., TRIPLETT, A., BERGMAN, L. & VAKAKIS, A. (2011) Energy harvesting from impulsive loads using intentional essential nonlinearities. *ASME J. Vib. Acoust.* **133**, 011001.

[23] ROUNDY, S. & QUINN, D. (2005) On the effectiveness of vibration-based energy harvesting. *J. Intell. Mater. Syst. Struct.* **16**, 809–823.

[24] ROUNDY, S. & WRIGHT, P. (2004) A piezoelectric vibration based generator for wireless electronics. *Smart Mater. Struct.* **13**, 1131–1142.

[25] SEBALD, G., KUWANO, H., GUYOMAR, D. & DUCHARNE, B. (2011) Experimental Duffing oscillator for broadband piezoelectric energy harvesting. *Smart Mater. Struct.* **20**, 102001.

[26] SEBALD, G., KUWANO, H., GUYOMAR, D. & DUCHARNE, B. (2011) Simulation of a Duffing oscillator for broadband piezoelectric energy harvesting. *Smart Mater. Struct.* **20**, 075022.

[27] SODANO, H., INMAN, D. & PARK, G. (2004) A review of power harvesting from vibration using piezoelectric materials. *Shock Vib. Dig.* **36**, 197–205.

[28] SODANO, H., INMAN, D. & PARK, G. (2005) Generation and storage of electricity from power harvesting devices. *J. Intell. Mater. Syst. Struct.* **16**, 67–75.

[29] SODANO, H., PARK, G., LEO, D. & INMAN, D. (2003) Use of piezoelectric energy harvesting devices for charging batteries. In: *Proc. SPIE 5050, Smart Structures and Materials 2003: Smart Sensor Technology and Measurement Systems*, SPIE, The International Society for Optics and Photonics, Bellingham, WA, pp. 101.

[30] STANTON, S., MCGEHEE, C. & MANN, B. (2010) Nonlinear dynamics for broadband energy harvesting: investigation of a bistable piezoelectric inertial generator. *Physica D* **239**, 640–653.

[31] YANG, X. & DEB, S. (2013) Multiobjective cuckoo search for design optimization. *Comp. Oper. Res.* **40**, 1616–1624.